JCTC Journal of Chemical Theory and Computation

Article

pubs.acs.org/JCTC

Transient Effects of Excluded Volume Interactions on the Translational Diffusion of Hydrodynamically Anisotropic Molecules

Maciej Długosz*

Center of New Technologies, University of Warsaw, Żwirki i Wigury 93, Warsaw 02-089, Poland

Jan M. Antosiewicz

Department of Biophysics, Faculty of Physics, University of Warsaw, Żwirki i Wigury 93, Warsaw 02-089, Poland

ABSTRACT: We have investigated effects of excluded volume interactions on the translational diffusion of hydrodynamically anisotropic molecules. For that, we have performed rigid-body Brownian dynamics simulations of aqueous solutions of hen egg-white lysozyme (HEWL), at concentrations ranging from 1.25 mg/mL to 250 mg/mL and evaluated the lysozyme's self-diffusion. In the long time limit (above 1 μs), the protein's translational diffusion is isotropic, regardless the solution concentration. However, on the time scale of the order of up to hundreds of nanoseconds, the anisotropic translational diffusion is observed, with the transition time from the anisotropic to isotropic translational diffusion depending on the lysozyme concentration. The magnitude of the translational diffusion anisotropy in this transient regime is also concentration-dependent and steric interactions enhance the anisotropy. Moreover, steric interactions cause the anisotropy to be a nonmonotonic function of time. When the hydrodynamic anisotropy of the protein is neglected in Brownian dynamics simulations and its diffusion tensor is replaced with average translational and rotational diffusion coefficients, the lysozyme's translational dynamics in the long-time limit is similar to that in the case of the corresponding hydrodynamically anisotropic object. However, such a similarity is not observed below 1 μs and in this time regime the translational dynamics of lysozyme molecules modeled with isotropic diffusion coefficients substantially deviates from that derived from Brownian dynamics simulations of their hydrodynamically anisotropic counterparts.

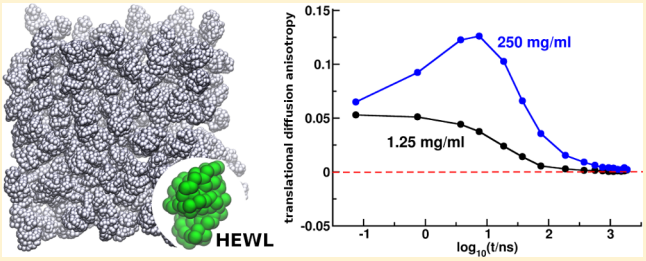

1. INTRODUCTION

Processes that occur in nature at low Reynolds numbers are governed predominantly by diffusion.[1] As an example, one may consider the formation of macromolecular complexes that involves at least two stages.[2,3] During the first stage, macromolecules search for reaction partners via the translational and rotational diffusion. At the end of this stage, the two binding partners reach a configuration resembling the one observed in their functional complex: a so-called encounter complex.[4] In the second stage, specific short-range interactions and intermolecular contacts are established and then further steps, e.g., a chemical reaction, possibly follow. During the first stage shapes of macromolecules may play a role, both in their bulk hydrodynamic diffusion as well as upon the encounter complex formation. Shapes of typical biomolecules deviate from spherical, and thus, Brownian motions of asymmetric or at least anisotropic particles are of significant interest in molecular biophysics.[5−8]

In the long-time limit, the unrestricted translational diffusion of a particle that undergoes translational and rotational Brownian motions, when evaluated in some laboratory coordinate system, is isotropic, regardless of the particle's shape. As a consequence, it is often assumed that molecular shapes can be ignored, which enables efficient simulations of translational diffusion in complex, multicomponent biological systems with a single sphere assigned to each molecule in the studied ensemble.[5,9−11] Another approach encountered in modeling of translational diffusion of biomolecules retains in simulations geometric details of the particles but ignores their hydrodynamic anisotropies, i.e. average diffusion coefficients of biomolecules are used instead of anisotropic diffusion tensors.[12−14] Both approaches assume that, regardless of the time scale, the diffusion of biomolecules can be described with the mathematical formalism valid for spherical Brownian particles.

However, it is well-known[15] that for a free, axially symmetric Brownian particle, like an ellipsoid or a cylinder, the dependence of the instantaneous translational diffusion on the current orientation of the particle leads to transiently anisotropic translational motion. Thus, such a particle exhibits the anisotropic translational diffusion for short and moderate times, which changes to isotropic at long times, as the rotational diffusion eventually washes out the dependence of the

Received: February 13, 2014
Published: May 1, 2014

translational motion of the particle on its initial orientation;[15,16] the long-time translational diffusion coefficient is an average over the three diagonal elements of the translational diffusion tensor of the particle. Similar behavior is expected for fully asymmetric particles such as biomolecules, and what is really interesting and has not been systematically studied yet, is how molecular crowding encountered in living cells affect this transient behavior of the translational dynamics of asymmetric molecules.

In the current work, we investigate effects exerted by molecular crowding on translational diffusion of hydrodynamically anisotropic molecules at different time scales. With the focus of our study being on shape-related effects, and because we are not interested in absolute values of diffusion coefficients, the only intermolecular interaction that we take into account is the excluded volume effect. As our model systems, we consider monodisperse solutions of hen egg white lysozyme (HEWL) proteins (see Figure 1). We apply a rigid-body Brownian dynamics approach[17−20] that accurately accounts for hydrodynamic anisotropies of geometrically detailed diffusing objects to characterize the translational dynamics of HEWL particles at concentrations of up to 250 mg/mL.

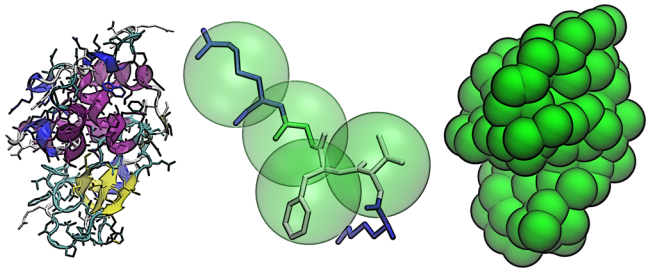

Figure 1. (Left) Structure of hen egg-white lysozyme, HEWL (PDB ID: 6LYZ).[29] (Center) Residue-based hydrodynamic modeling of the HEWL molecule. (Right) Hydrodynamic model of HEWL. [Drawings were done using the VMD package.[30]]

We have found that, while above 1 μs, HEWL's translational diffusion is isotropic, regardless of the solution concentration, on the time scale of the order of up to a few hundred nanoseconds, anisotropic translational diffusion is observed, with the transition time from the anisotropic to isotropic translational diffusion that depends on the concentration of lysozyme molecules. The magnitude of the translational diffusion anisotropy in this transient regime is also concentration-dependent. Steric interactions enhance the anisotropy and overall larger anisotropy is observed at higher lysozyme concentrations. Moreover, in the case of concentrated solutions, the transient anisotropy is a nonmonotonic function of time. When the hydrodynamic anisotropy of HEWL is neglected in Brownian dynamics simulations and its diffusion tensor is replaced with isotropic translational and rotational diffusion coefficients (but with HEWL molecules modeled with the full geometric detail), the lysozyme's translational dynamics in the long-time limit is similar to that observed in the case of the corresponding hydrodynamically anisotropic object. However, such a similarity is not observed below 1 μs. In this time regime the translational dynamics of lysozyme molecules modeled with isotropic diffusion coefficients deviates from that derived from Brownian dynamics simulations of their hydrodynamically anisotropic counterparts.

We argue that the diffusional behavior of arbitrarily shaped particles that we observe on the submicrosecond time scale might be of biological importance, particularly when the formation of molecular complexes is considered.

2. METHODS

2.1. Diffusion Tensor of a Rigid Macromolecule. Diffusional motions (translations and rotations) of rigid molecules in dilute solutions are governed by their diffusion tensors, 6 × 6 matrices that can be partitioned to four 3 × 3 blocks related to translational (*trans*) and rotational (*rot*) diffusivities and their couplings (*trans-rot* and *rot-trans*):[18,21]

$$\mathbf{D}_{6\times6} = \begin{pmatrix} \mathbf{D}^{trans} & \mathbf{D}^{trans\text{-}rot} \\ \mathbf{D}^{rot\text{-}trans} & \mathbf{D}^{rot} \end{pmatrix} \tag{1}$$

Translational and rotational diffusion coefficients in dilute solutions are given by

$$D_o^{trans} = \frac{1}{3}\mathrm{Tr}(\mathbf{D}^{trans}) \tag{2}$$

$$D_o^{rot} = \frac{1}{3}\mathrm{Tr}(\mathbf{D}^{rot}) \tag{3}$$

The diffusion tensor, particularly its translational and translation−rotation (rotation−translation) coupling blocks, depends on the origin. When the origin is located at the particle's center of diffusion (CD),[22,23] the coupling blocks become symmetric (the translation block is symmetric, regardless of the choice of the origin) and the translational diffusion coefficient (eq 2) reaches a minimum. Moreover, the diagonalization of the always-symmetric $\mathbf{D}^{rot}$ subtensor leads to the three eigenvalues and the three orthogonal principal axes. In this work, we assume that these axes form the particle coordinate system with the origin located at the CD.

Diffusion tensors of macromolecules can be obtained from rigid-body hydrodynamic calculations performed for atomistically detailed molecular models.[23−25]

Since, in this work, we are concerned directly only with the translational motion of molecules, we will omit the *trans* superscript in all further references to translational diffusion coefficients.

2.2. Rigid-Body Brownian Dynamics. *2.2.1. Propagation Algorithm.* Introducing the particle coordinate system (PCS), whose main axes coincide with the principal axes of particle's diffusional rotations and whose origin is located at the particle's CD, one may write the following propagation scheme for a rigid body of an arbitrary shape:[17,18,26]

$$\Delta\vec{x} = \frac{\Delta t}{k_B T}\mathbf{D}_{6\times6}\vec{M} + \vec{R}(\Delta t) \tag{4}$$

where $\vec{x} = (\vec{r}, \vec{\phi})^T$ is the vector describing the position of the CD ($\vec{r}$) and orientation ($\vec{\phi}$) of the molecule, $\mathbf{D}_{6\times6}$ is the 6 × 6 diffusion tensor of the molecule in the dilute solution (eq 1) evaluated in the PCS and constant during the simulation, Δt is the time step, and $\vec{M}$ is the generalized force vector accommodating forces and torques resulting from intermolecular interactions referred to the CD. The last term in the above equation, $\vec{R}(\Delta t)$, is a random displacement vector mimicking the Brownian noise, with zero mean and variance−covariance given with

$$\langle \vec{R}(\Delta t)\vec{R}^{T}(\Delta t)\rangle = 2\mathbf{D}_{6\times 6}\Delta t \quad (5)$$

evaluated via the Cholesky decomposition of the diffusion tensor.[26] Time-dependent position and orientation of the molecule in the laboratory coordinate system (LCS) are obtained by applying at each step of the simulation transformations between PCS and LCS.[18]

2.2.2. Model of the HEWL Protein. The rigid-body diffusion tensor of HEWL in the dilute solution was evaluated as described elsewhere.[27,28] Bead representation of the HEWL molecule was created, with spherical frictional elements positioned at geometric centers of its amino acids (see Figure 1). Each frictional element was assigned a radius computed as the mean maximal distance of any heavy atom of a given amino acid from the center of its bead, increased by the radius of a water molecule (1.4 Å). The resulting model of HEWL consisted of 129 beads with radii of 4.24 Å (see Figure 1). The diffusion tensor of this rigid conglomerate of spherical frictional elements was then evaluated using well-established techniques,[24,31] with the temperature set to 298 K and the solvent viscosity set to 0.01 P. In Table 1, diagonal entries of the translation block ($\mathbf{D}^{trans}$, eq 1) of the HEWL's diffusion tensor resulting from our calculations are given (eigenvalues of the $\mathbf{D}^{rot}$ block of $\mathbf{D}_{6\times 6}$, that correspond to diffusional rotations around the principal axes x, y, and z, are 16.8×10^{-3} (1/ns), 17.2×10^{-3} (1/ns), and 22.4×10^{-3} (1/ns)).

Table 1. Diagonal Entries of the HEWL's Translational Diffusion Tensor in the Dilute Solution ($D_{o,i\in x,y,z}$); HEWL's Translational Diffusion Coefficient in the Dilute Solution Is Denoted by D_o

$D_{o,x}$ [Å²/ns]	$D_{o,y}$ [Å²/ns]	$D_{o,z}$ [Å²/ns]	$D_o = (D_{o,x} + D_{o,y} + D_{o,z})/3$
11.47	11.72	12.67	11.96

The same bead representation of HEWL (Figure 1) was used in the modeling of excluded volume interactions between proteins. Excluded volume interactions between beads i and j (separated by the distance r_{ij}) that belong to different HEWL molecules are evaluated as a negative gradient of the following potential:

$$U_{ij}^{exc} = 4\varepsilon\left[\left(\frac{2\sigma}{r_{ij}}\right)^{12} - \left(\frac{2\sigma}{r_{ij}}\right)^{6}\right] \quad (6)$$

where σ is set to 4.24 Å and ε is set to k_BT (k_B is the Boltzmann constant and T the temperature). With the interbead cutoff of $2^{1/6}(2\sigma)$, only the short-range repulsion between beads is taken into account.

2.2.3. Simulations Setup. Rigid-body Brownian dynamics simulations were performed with the BD_BOX package.[19,20,32] Four HEWL systems were considered. Each system consisted of 220 HEWL molecules, that, at the beginning, were positioned and oriented randomly in a cubic cell. We considered four HEWL concentrations: 1.25, 10.0, 150.0, and 250.0 mg/mL. These were achieved by varying the volume of the simulation cell from $(1612\ Å)^3$ to $(275\ Å)^3$. Resulting occupied volume fractions (computed using the equivalent Stokes radius of HEWL) in the simulated systems were between 0.1% and 27%. All systems were simulated under periodic boundary conditions via the minimum image convention. While all of the systems were simulated using the fully anisotropic diffusion tensor of HEWL, for the most concentrated systems, we also performed BD simulations assigning HEWL molecules isotropic diffusion tensors (i.e., we used average translational and rotational diffusion coefficients instead of the full diffusion tensor, eqs 2 and 3), but with intermolecular interactions considered with the full geometric detail.

Apart from the HEWL systems described above, we have also simulated a solution of spherical particles of radii equivalent to the Stokes radius of HEWL: this system consisted of 220 spheres with radii of 18.3 Å, in the cubic cell of volume of $(275\ Å)^3$ (corresponding to the concentration of HEWL equal to 250 mg/mL).

In all simulations, only excluded volume interactions between particles were taken into account.

For each system, a single 70-μs BD simulation was performed. Each simulation was preceded by an equilibration stage with a duration of 1.5 μs, during which the studied systems were allowed to relax from their initial state. Temperature was set to 298 K. The simulation time step was set to 0.75 ps. Snapshots were collected from BD trajectories every 75 ps.

Even though the time step that we use to generate BD trajectories is relatively small and short-range repulsive forces are taken into account, a fraction of simulation steps may result in nonphysical overlaps between some of the particles. This is a consequence of the random term in the equation of motions (eq 4). To avoid such situations, after a BD step is made, we examine the resulting configuration of molecules in the simulated system for overlaps. If they are detected, all particles are brought back to the previous configuration and a BD step is attempted with different random vectors until there are no overlaps in the system.

2.3. Evaluation of HEWL's Translational Diffusion. Translational diffusion properties of HEWL are evaluated using the mean square displacement of its CD, $\langle \delta r^2 \rangle$. The translational diffusion coefficient of HEWL at a given time, $D(\delta t)$, is estimated based on the relation

$$\langle (\delta r(\delta t))^2 \rangle = 6D(\delta t)\delta t \quad (7)$$

with

$$\delta r(\delta t) = [(\vec{r}(t+\delta t) - \vec{r}(t))\cdot(\vec{r}(t+\delta t) - \vec{r}(t))]^{1/2} \quad (8)$$

where $\vec{r} = (r_x, r_y, r_z)$ denotes the position of the CD of a given HEWL molecule in the LCS, δt is the observation interval, and $\langle\cdot\rangle$ indicates an average over the choice of the initial state of a particular molecule and over the ensemble of molecules.

Evaluation of HEWL's translational diffusion anisotropy is based on the approach depicted schematically in Figure 2. Vector of the translation of the CD of a given particle during a given interval δt—between time t and time $(t + \delta t)$—evaluated in the LCS is projected on axes of the PCS whose position and orientation in the LCS are taken at time t. The three translational diffusion coefficients corresponding to the directions of the principal axes of the particle's rotations, $D_{i\in(x,y,z)}(\delta t)$, then are evaluated using the following relationship:

$$\langle (\delta r_{i\in(x,y,z)}(\delta t))^2 \rangle = 2\delta t D_i(\delta t) \quad (9)$$

where

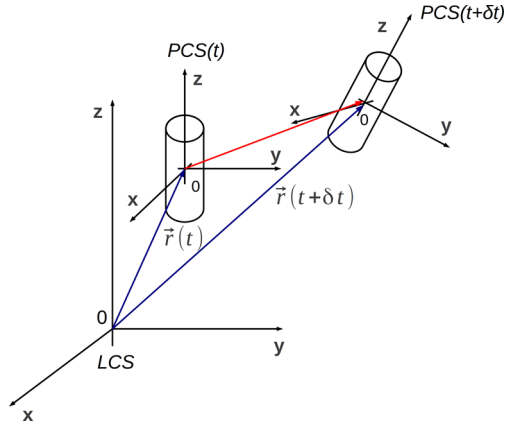

Figure 2. Evaluation of $D_{i\in x,y,z}(\delta t)$; the vector describing (in the laboratory coordinate system, LCS) the translation of the particle's center of diffusion (red arrow) during a given interval δt is projected on axes of the particle coordinate system, PCS(t), oriented in the LCS at the beginning of the considered translation (at time t). Coordinates of the translation vector in the PCS(t) are then used to derive values of $D_{i\in x,y,z}(\delta t)$, according to eqs 9 and 10.

$$\delta r_{i\in(x,y,z)}(\delta t) = [(r_i(t+\delta t) - r_i(t))\cdot(r_i(t+\delta t) - r_i(t))]^{1/2} \quad (10)$$

denotes the three components of the translation vector in the PCS at time t (see Figure 2). The time-ensemble average is denoted by $\langle\cdot\rangle$.

Translational diffusion anisotropy, $\Delta(\delta t)$, is evaluated as

$$\Delta(\delta t) = \sqrt{\frac{1}{2}} \times \sqrt{\frac{(D_x(\delta t) - D_y(\delta t))^2 + (D_x(\delta t) - D_z(\delta t))^2 + (D_y(\delta t) - D_z(\delta t))^2}{(D_x(\delta t))^2 + (D_y(\delta t))^2 + (D_z(\delta t))^2}} \quad (11)$$

In the infinite dilution limit, HEWL's translational diffusion anisotropy at $\delta t = 0$, Δ_∞, resulting from eigenvalues of its translational diffusion tensor (Table 1), is 0.053.

In addition, the integral

$$\chi = \int_0^\infty \Delta(\delta t)\delta t \quad (12)$$

is used to quantify the translational diffusion anisotropy at different concentrations. In practice, the upper boundary of the above integral is set to 1.5 μs.

3. RESULTS

3.1. HEWL's Translational Diffusion in LCS. In Figure 3, we show the mean square displacement (normalized via the value of the HEWL's dilute-solution translational diffusion coefficient, D_o in Table 1), $\langle\delta r^2\rangle$, of the HEWL's CD, measured in the laboratory coordinate system, as a function of the observation interval δt.

The clear variation of $\langle\delta r^2\rangle$ with δt that is seen for concentrated solutions (ρ = 150 mg/mL, 250 mg/mL) of HEWL proteins and their equivalent spheres (ρ = 250 mg/mL) (see Figure 3) is indicative of the anomalous subdiffusion, i.e., a diffusion process with a nonlinear relationship to time, resulting from the fact that molecules act over short distances as obstacles for each other.[33−36] However, as the observation interval δt increases above ∼10 ns, normal diffusion is

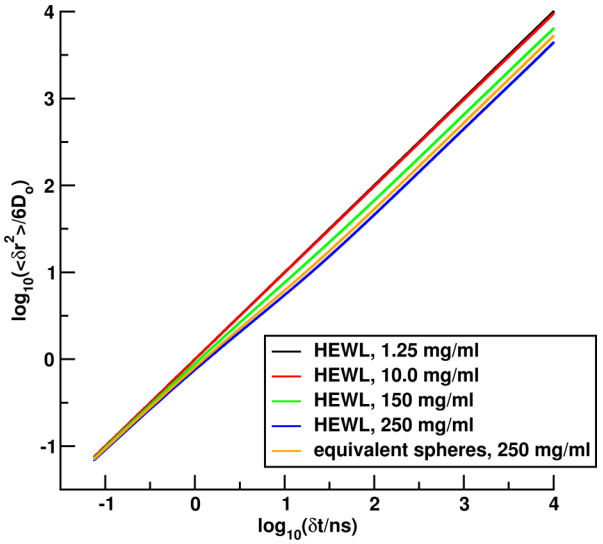

Figure 3. Normalized mean square displacement ($\langle\delta r^2\rangle$) as a function of the interval δt (eq 8). Plots have been derived from Brownian dynamics simulations of HEWL solutions at different concentrations. A similar plot, derived from BD simulations of the solution of equivalent Stokes spheres at 250 mg/mL, is shown for comparison. Plots are normalized via the value of the dilute-solution translational diffusion coefficient of HEWL (see Table 1).

recovered. Considering average translational diffusion coefficients derived based on the asymptotic behavior of $\langle\delta r^2\rangle$ plots (eq 7), we conclude that HEWL's diffusion at 250 mg/mL, when compared with the diffusion in the dilute solution, is slowed by 55% in the case of hydrodynamically anisotropic proteins modeled with full geometric detail and by 48% when HEWL molecules are modeled as equivalent Stokes spheres. Thus, the effective radius of HEWL in concentrated solution should be set to a slightly larger value than the one resulting from the evalution of HEWL's dilute solution properties, to account for HEWL's nonspherical shape and, thus, its nonisotropic steric interactions with surrounding molecules. Obviously, changes in the translational diffusion reported above that result solely from excluded volume interactions between simulated particles, are much smaller than those observed in experiments, where translational diffusion coefficients of probe proteins measured in cytosol-like systems are reduced by a factor of ∼10 or even more in comparison with dilute solution values.[37−39] However, at this point, we again stress that we are not interested in the quantitative prediction of HEWL's translational diffusion coefficients, which is a goal that would require a detailed modeling of direct intermolecular interactions, as well as solvent-mediated hydrodynamic interactions between diffusing molecules.[5,6,39]

3.2. HEWL's Translational Diffusion over Different Time Scales. Applying the procedure summarized in Figure 2, we have evaluated translational diffusion coefficients, $D_{i\in(x,y,z)}$, of HEWL that are derived from the components of the CD translation that occurs during the observation interval δt, evaluated in the PCS at the beginning of the observation. Values of $D_{i\in(x,y,z)}$, obtained for different HEWL concentrations, are plotted in Figure 4, as functions of the observation interval δt. As expected, for a given HEWL concentration, when δt converges to zero, all $D_{i\in x,y,z}$ converge to eigenvalues of HEWL's dilute-solution translational diffusion tensor (Table 1), regardless of the concentration of HEWL solutions, which is a

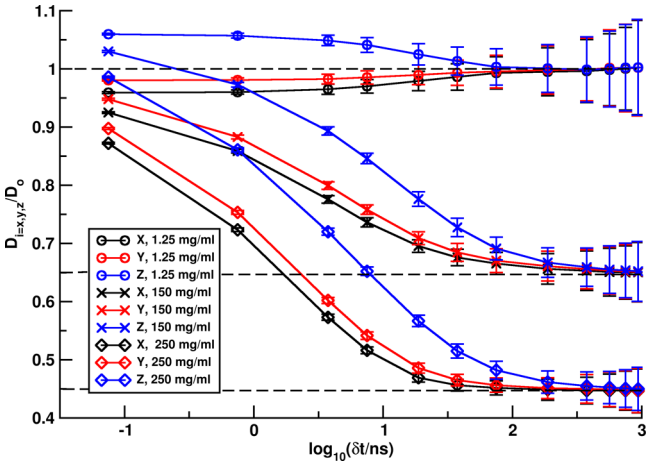

Figure 4. $D_{i\in x,y,z}$ as a function of the interval δt for HEWL solutions at different concentrations. Values of $D_{i\in x,y,z}$ are normalized via the value of the HEWL's dilute-solution translational diffusion coefficient (see Table 1).

consequence of the fact that hydrodynamic interactions, and particularly their short-range, many-body components, are omitted in our simulations. When δt increases, differences between values of $D_{i\in x,y,z}$ decrease as the rotational diffusion of molecules causes eventually the averaging of translations in different directions. Thus, the translational diffusion of HEWL, which is clearly anisotropic when small values of δt are considered, becomes isotropic for sufficiently large values of the observation interval. Tables 2 and 3, contain values of $D_{i\in x,y,z}$

Table 2. Values of $D_{i\in x,y,z}$ for δt = 0.075 ns Obtained from BD Simulations of HEWL Solutions

ρ [mg/mL][a]	$D_x \pm \sigma_x$ [Å^2/ns]	$D_y \pm \sigma_y$ [Å^2/ns]	$D_z \pm \sigma_z$ [Å^2/ns]
1.25	11.47 ± 0.02	11.72 ± 0.02	12.67 ± 0.02
10.0	11.45 ± 0.02	11.71 ± 0.02	12.65 ± 0.02
150.0	11.05 ± 0.02	11.33 ± 0.02	12.31 ± 0.02
250.0	10.43 ± 0.02	10.73 ± 0.02	11.78 ± 0.02
250.0$^{\text{isotropic}}$	10.83 ± 0.02	10.92 ± 0.02	11.16 ± 0.02

[a]The superscript "isotropic" indicates the results of the BD simulation in which HEWL molecules are described with isotropic diffusion tensors.

Table 3. Limiting Values of $D_{i\in x,y,z}$ Obtained from BD Simulations of HEWL Solutions

ρ [mg/mL][a]	$D_x \pm \sigma_x$ [Å^2/ns]	$D_y \pm \sigma_y$ [Å^2/ns]	$D_z \pm \sigma_z$ [Å^2/ns]	$(D_x + D_y + D_z)/(3D_o)$[b]
1.25	11.97 ± 0.97	11.97 ± 0.98	11.98 ± 0.98	1.00
10.0	11.63 ± 0.96	11.63 ± 0.99	11.61 ± 0.98	0.97
150.0	7.77 ± 0.61	7.78 ± 0.55	7.79 ± 0.61	0.65
250.0	5.33 ± 0.45	5.34 ± 0.46	5.37 ± 0.44	0.45
250.0$^{\text{isotropic}}$	5.32 ± 0.41	5.32 ± 0.41	5.34 ± 0.41	0.45

[a]The superscript "isotropic" indicates the results of the BD simulation in which HEWL molecules are described with isotropic diffusion tensors. [b]D_o denotes the dilute-solution translational diffusion coefficient of the HEWL.

obtained for different HEWL concentrations for intervals δt equal to 0.075 and 1500 ns, respectively. In addition, values of $D_{i\in(x,y,z)}$ derived from the BD simulation of HEWL molecules modeled with isotropic diffusion coefficients (ρ = 250 mg/mL) are given. For the observation interval equal to 0.075 ns, these values deviate from those derived from the simulation of hydrodynamically anisotropic HEWL molecules (see Table 2). Moreover, even though for δt = 0, translational diffusion of hydrodynamically isotropic HEWLs is isotropic, with δt increasing to 0.075 ns, anisotropic translational diffusion is observed, as a consequence of the anisotropic shape of HEWL and thus its anisotropic steric interactions with other proteins. In the log-time limit, values of $D_{i\in(x,y,z)}$ obtained from simulations of hydrodynamically isotropic HEWLs are in agreement with those obtained from the BD simulation of hydrodynamically anisotropic HEWLs.

Translational dynamics of HEWL over different time scales can be characterized by plotting $\Delta(\delta t)$ functions defined by eq 11. This is done in Figure 5.

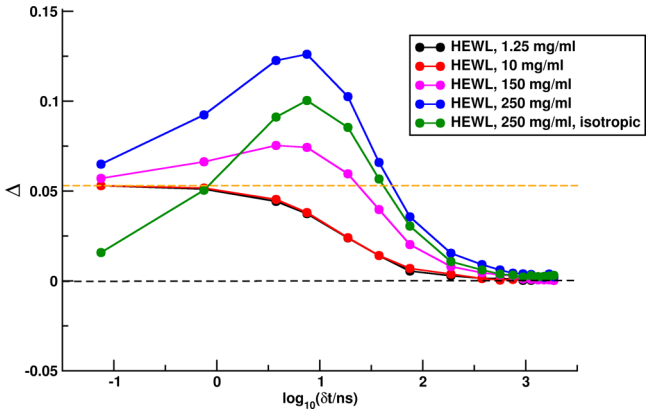

Figure 5. Dependency of the anisotropy Δ on the interval δt (see eq 11) for different concentrations of HEWL molecules. The superscripted word "isotropic" denotes results of BD simulations of HEWL molecules that are assigned isotropic diffusion tensors of the equivalent sphere. The orange dashed line denotes the value of anisotropy computed based on the entries of the HEWL's dilute-solution diffusion tensor (Table 1), Δ_∞.

For the most dilute solution that we have studied (ρ = 1.25 mg/mL), HEWL's translational diffusion anisotropy measured by Δ is a monotonic function of the observation interval. When δt converges to zero, Δ converges to the value of 0.053 (Δ_∞), which can be predicted based on the diagonal entries of the HEWL's dilute-solution translational diffusion tensor (Table 1). With the increasing δt, Δ monotonically decreases to zero. Similar behavior is characteristic for the $\Delta(\delta t)$ plot obtained for the HEWL solution at a concentration of 10 mg/mL (Figure 5). However, more-complicated behavior is observed at higher HEWL concentrations (150 mg/mL and 250 mg/mL), where functions $\Delta(\delta t)$ are no longer monotonic (Figure 5). Starting from Δ_∞ (for δt converging to zero), they initially increase with the increasing observation interval, reach a maximal value, and then decrease to zero for sufficiently large δt. The largest anisotropy is observed in the case of the most dense HEWL solution. Clearly, the magnitude of the transiently observed HEWL's translational diffusion anisotropy is an increasing function of the HEWL concentration.

In Figure 5, we also show the plot of $\Delta(\delta t)$ derived from the simulation in which HEWL molecules were assigned isotropic diffusion coefficients. In this case, a nonmonotonic behavior is also visible: being initially zero, Δ increases with the increasing δt reaches a maximum and again drops to zero. Magnitude of the anisotropic effect is however smaller than that observed for

dx.doi.org/10.1021/ct500124r | J. Chem. Theory Comput. 2014, 10, 2583−2590

the corresponding plot obtained from the BD simulation of hydrodynamically anisotropic HEWL molecules (Figure 5).

Interestingly, the time characterizing the transition from the anisotropic to isotropic diffusion depends on the HEWL concentration (Table 4). After the initial increase, the dilute-

Table 4. Estimation of HEWL's Transition Times from Anisotropic to Isotropic Translational Diffusion at Different Concentrations

ρ [mg/mL]	$T_{\Delta(\delta t=0)\rightarrow 1.0\times\Delta_\infty}$ [ns]	$T_{\Delta(\delta t=0)\rightarrow 0.1\times\Delta_\infty}$ [ns]
1.25	n/a	97
10.0	n/a	146
150.0	27	352
250.0	57	677

solution value of anisotropy, Δ_∞, is recovered after 27 ns in the case of the HEWL solution at the concentration of 150 mg/mL, and after 57 ns in the case of the HEWL solution at the concentration of 250 mg/mL ($T_{\Delta(\delta t=0)\rightarrow 1.0\times\Delta_\infty}$, Table 4). In the case of the most dilute solution (ρ = 1.25 mg/mL), anisotropy drops to 10% of the initial value (Δ_∞) after 97 ns ($T_{\Delta(\delta t=0)\rightarrow 0.1\times\Delta_\infty}$, Table 4). As the HEWL concentration increases, the value of $T_{\Delta(\delta t=0)\rightarrow 0.1\times\Delta_\infty}$ also increases, up to nearly 700 ns in the case of the most concentrated HEWL solution that we have considered.

Integrals χ (eq 12), the values of which are dependent both on the magnitude of the anisotropy as well as the duration of the transition from anisotropic to isotropic diffusion, can be used to quantify the anisotropic effect observed in the transient regime. Their values, given in Table 5, clearly indicate that the

Table 5. Values of Integrals $\int_0^\infty \Delta(\delta t)\delta t$ Obtained for Different Concentrations of HEWL Proteins

ρ [mg/mL][a]	$\chi = \int_0^\infty \Delta(\delta t)\delta t$ [ns]
1.25	3.3
10.0	3.9
150.0	8.2
250.0	15.7
$250.0^{\text{isotropic}}$	12.0

[a]The superscript "isotropic" indicates the results of the BD simulation in which HEWL molecules are described with isotropic diffusion tensors.

anisotropic effect is dependent on the solution concentration and increases as the role of steric interactions increases. The value of χ obtained for the concentration of 250 mg/mL is ~5 times larger than the value of χ obtained for the dilute solution. The fact that steric interactions enhance translational diffusion anisotropy is also evident if one considers the value of χ that corresponds to the BD simulation in which described with full geometric detail HEWL molecules were assigned isotropic diffusion coefficients (Table 5). In this case, the anisotropy observed in the transient regime results solely from steric interactions between particles. However, the χ integral resulting from the BD simulation of hydrodynamically isotropic HEWL molecules is ~30% smaller than the integral obtained from the corresponding simulation of hydrodynamically anisotropic molecules. This is an indication that the problem of the translational dynamics of HEWL molecules in the concentrated solution can be addressed only partially, when isotropic diffusion coefficients are used instead of fully anisotropic diffusion tensors in BD simulations.

4. DISCUSSION

We have shown that the well-recognized transient anisotropy[15] of the translational diffusion of an anisotropic particle is substantially enhanced in crowded solutions. Introducing as measures of the translational diffusion anisotropy, the parameter Δ (eq 11) and its integral over time, χ (eq 12), we observed that the magnitude of the anisotropy is several times larger in crowded solutions, when compared to infinitely diluted solutions (see Table 5). In addition, the transient anisotropy lasts longer when the degree of crowding is larger (Table 4).

One may ask whether the enhancement of the translational diffusion anisotropy that we observe in concentrated HEWL solutions (150 mg/mL and 250 mg/mL) on the time scale below 1 μs, is of any biological relevance. Trying to address such a question, we have studied the bimolecular encounter in the monodisperse solution of spheres of radii (R) equal to 18.3 Å (Stokes radius of the HEWL molecule) with the concentration of 250 mg/mL. Defining an encounter as the situation where the center-to-center distance within a given pair of spheres is smaller than $2R$ + 5 Å, we determined association times for different initial center-to-center distances of several spheres ($4R$, $6R$, $8R$). In addition, we also determined dissociation times, i.e., times needed for the two spheres, which are initially separated by $2R$ + 5 Å, to reach a given center-to-center separation ($4R$, $6R$, $8R$). Distributions of association and dissociation times that we obtained are given in Figure 6. When the initial (or final) separation distance is

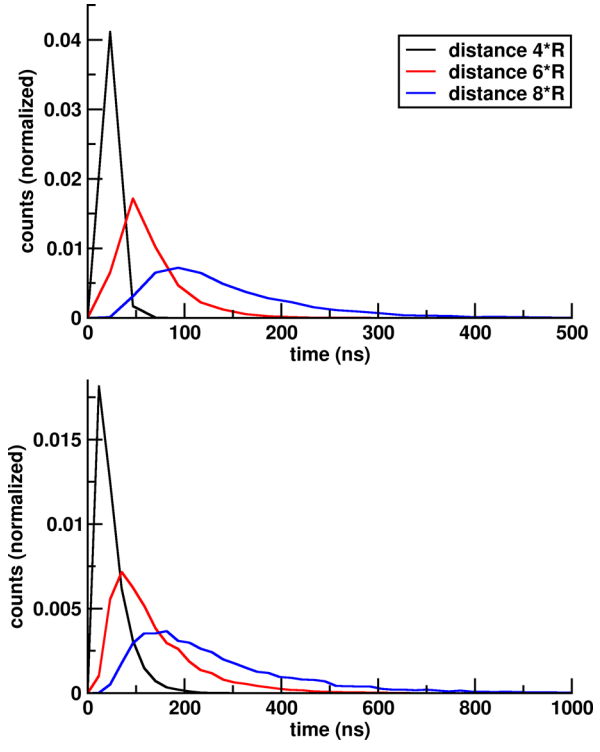

Figure 6. Distributions of association (top) and dissociation times (bottom) obtained for different values of the separation criterion from the BD simulation of spherical HEWL particles at the concentration of 250 mg/mL. See text for details.

dx.doi.org/10.1021/ct500124r | J. Chem. Theory Comput. 2014, 10, 2583−2590

increased, distributions of association (or dissociation) times become wider, and their maxima shift toward longer times (Figure 6). In addition, for a particular value of the final (initial) separation, dissociation times are overall longer than association times. This results from the fact that, before the assumed separation distance is achieved by the two particles initially forming an encounter complex, their re-encounters are possible. What is important is that all times in Figure 6 are below 1 μs, in the regime where anisotropic translational diffusion is observed. Separations considered (Figure 6) are below 150 Å, which is substantially less than the average dimensions of a typical bacterial (1 μm) or eukaryotic cell (10 μm). Moreover, the diffusional search for reaction partners taking place inside living cells (e.g., in their cytoplasm) certainly takes longer than 1 μs. While long-time isotropic diffusion enables molecules to explore their surroundings in a uniform manner, increasing their chances to find themselves tens or hundreds angstroms from their binding partners, the short-time anisotropic translational diffusion might increase the probability of the formation of their complex once the binding parters are in vicinity of each other.

Considering the dissociation process, the enhanced anisotropy of the translational diffusion might increase the chances of the complexed binding partners separating, because of the faster movement in a particular direction. Enhanced anisotropy may also play role by increasing the number of re-encounters of molecules that occur after an encounter that does not lead to the formation of the functional complex.

We thus argue that the existence of the two time scales—the short one that, in the studied system, is on the order of up to hundreds of nanoseconds, and the long one that in the studied system is above a microsecond—is biologically meaningful.

Since the only intermolecular interaction taken into account in the present work is the excluded volume effect, we should also comment on possible changes to the picture emerging from our work that would result from the inclusion of electrostatic and, perhaps more importantly, hydrodynamic interactions. Both these interactions are bound to play a role in the bulk diffusion of molecules, as well as during their diffusional encounters. Because these interactions are long-range, they introduce correlations between positions and velocities of proteins, affect relaxation times characterizing local changes of the surroundings of a given lysozyme molecule, and therefore modify its translational and rotational dynamics. The question whether the dependencies shown in Figure 5 would be qualitatively changed by these interactions is not easy to answer, since the rigorous treatment of hydrodynamic interactions in rigid-body Brownian dynamics simulations does not seem to be possible at present. The reason is that while, in principle, there exists methods and tools accounting for the long-range and the many-body character of hydrodynamic interactions, as well as complicated proteins' shapes that are based either on hydrodynamic bead models[40−42] or on the boundary element approach,[43−46] their application to evaluate hydrodynamic interactions during BD simulations of concentrated, multicomponent solutions demands prohibitive computational costs.

AUTHOR INFORMATION

Corresponding Author

*Tel.: +48 22 5540 821. Fax: +48 22 5540 801. E-mail: mdlugosz@cent.uw.edu.pl.

Notes

The authors declare no competing financial interest.

ACKNOWLEDGMENTS

The authors acknowledge support from National Science Centre (No. N N519 646640). This research was supported in part by PL-Grid Infrastructure (ACK Cyfronet AGH).

REFERENCES

(1) Purcell, E. M. *Am. J. Phys.* **1977**, *45*, 3−11.
(2) Vijayakumar, M.; Wong, K. Y.; Schreiber, G.; Fersht, A. R.; Szabo, A.; Zhou, H. X. *J. Mol. Biol.* **1998**, *278*, 1015−1024.
(3) Shoup, D.; Szabo, A. *Biophys. J.* **1982**, *40*, 33−39.
(4) Spaar, A.; Dammer, C.; Gabdoulline, R. R.; Wade, R.; Helms, V. *Biophys. J.* **2006**, *90*, 1913−1924.
(5) Ando, T.; Skolnick, J. *Proc. Natl. Acad. Sci. U.S.A.* **2010**, *107*, 18457−18462.
(6) Rosen-Runge, F.; Henning, M.; Zhang, F.; Jacobs, R. M. J.; Sztucki, M.; Schober, H.; Seydel, T.; Schreiber, F. *Proc. Natl. Acad. Sci. U.S.A.* **2011**, *108*, 11815−11820.
(7) Fakhri, N.; MacKintosh, F. C.; Lounis, B.; Cognet, L.; Pasquali, M. *Science* **2010**, *330*, 1804−1807.
(8) Hanasaki, I.; Isono, Y. *Phys. Rev. E* **2012**, *85*, 051134.
(9) Dix, J. A.; Verkman, A. S. *Annu. Rev. Biophys.* **2008**, *37*, 247−263.
(10) Ridgway, D. *Biophys. J.* **2008**, *94*, 3748−3759.
(11) Bicout, D. J.; Field, M. J. *J. Phys. Chem.* **1996**, *100*, 2489−2497.
(12) McGuffee, S. R.; Elcock, A. H. *J. Am. Chem. Soc.* **2006**, *128*, 12098−12110.
(13) McGuffee, S. R.; Elcock, A. H. *PLoS Comput. Biol.* **2010**, *6*, e1000694.
(14) Mereghetti, P.; Wade, R. C. *J. Phys. Chem. B* **2012**, *116*, 8523−8533.
(15) Grima, R.; Yaliraki, S. N. *J. Chem. Phys.* **2007**, *127*, 084511.
(16) Schluttig, J.; Korn, C. B.; Schwarz, U. S. *Phys. Rev. E* **2010**, *81*, 030902(R).
(17) Allison, S. *Macromolecules* **1991**, *24*, 530−536.
(18) Fernandes, M. X.; García de la Torre, J. *Biophys. J.* **2002**, *83*, 3039−3048.
(19) Długosz, M.; Antosiewicz, J. J. *Chem. Theory Comput.* **2013**, *9*, 1667−1677.
(20) Długosz, M.; Antosiewicz, J. M. *J. Chem. Theory Comput.* **2014**, *10*, 481−491.
(21) Brenner, H. J. *Colloid. Sci.* **1965**, *20*, 104−122.
(22) Harvey, S. C.; García de la Torre, J. *Macromolecules* **1980**, *13*, 960−964.
(23) García Bernal, J. M.; García de la Torre, J. *Biopolymers* **1980**, *19*, 751−766.
(24) García de la Torre, J.; Bernadó, P.; Pons, M. *Methods Enzymol.* **2005**, *394*, 419−430.
(25) Carrasco, B.; García de la Torre, J. *Biophys. J.* **1999**, *76*, 3044−3057.
(26) Ermak, D. L.; McCammon, J. A. *J. Chem. Phys.* **1978**, *69*, 1352−1360.
(27) Antosiewicz, J. *Biophys. J.* **1995**, *69*, 1344−1354.
(28) Antosiewicz, J.; Porschke, D. *J. Phys. Chem.* **1989**, *93*, 5301−5305.
(29) Diamond, R. *J. Mol. Biol.* **1974**, *82*, 371−391.
(30) Humphrey, W.; Dalke, A.; Schulten, K. *J. Mol. Graphics* **1996**, *14*, 33−38.
(31) García de la Torre, J. *Biophys. Chem.* **2001**, *94*, 265−274.
(32) Długosz, M.; Zieliński, P.; Trylska, J. *J. Comput. Chem.* **2011**, *32*, 2734−2744.
(33) Saxton, M. J. *Biophys. J.* **1994**, *66*, 394−401.
(34) Weiss, M.; Elsner, M.; Kartberg, F.; Nilsson, T. *Biophys. J.* **2004**, *87*, 3518−3524.
(35) Banks, D. S.; Fradin, C. *Biophys. J.* **2005**, *83*, 2960−2971.
(36) Saxton, M. J. *Biophys. J.* **2007**, *92*, 1178−1191.

(37) Elowitz, M. B.; Surette, M. G.; Wolf, P. E.; Stock, J. B.; Leibler, S. *J. Bacteriol.* **1999**, *181*, 197−203.
(38) Konopka, M. C.; Shkel, I. A.; Cayley, S.; Record, M. T.; Weisshaar, J. C. *J. Bacteriol.* **2006**, *188*, 6115−6123.
(39) Wang, Y.; Li, C.; Pielak, G. J. *J. Am. Chem. Soc.* **2010**, *132*, 9392−9397.
(40) Cichocki, B.; Felderhof, B. U.; Hinsen, K.; Wajnryb, E.; Bławździewicz, J. *J. Chem. Phys.* **1994**, *100*, 3780−3790.
(41) Hinsen, K. *Comput. Phys. Commun.* **1995**, *88*, 327−340.
(42) Cichocki, B.; Hinsen, K. *Phys. Fluids* **1995**, *7*, 285−291.
(43) Youngren, G. K.; Acrivos, A. J. *Fluid Mech.* **1975**, *69*, 377−402.
(44) Wegener, W. A. *Biopolymers* **1986**, *25*, 627−637.
(45) Aragon, S. A. *J. Comput. Chem.* **2004**, *25*, 1191−1205.
(46) Aragon, S. R. *Methods* **2011**, *54*, 101−114.